Int. J. Solids Structures Vol. 31, No. 2, pp. 269–277, 1994
Printed in Great Britain

0020–7683/94 $6.00+ .00

A UNIFIED NUMERICAL APPROACH FOR THE ANALYSIS OF ROTATING DISKS INCLUDING TURBINE ROTORS

SUSANA C. STERNER and SUNIL SAIGAL
Department of Civil Engineering, Carnegie Mellon University, Pittsburgh, PA, U.S.A.

and

WALTER KISTLER
Worcester Polytechnic Institute, Worcester, MA, U.S.A.

and

DAVID E. DIETRICH
Swanson Analysis Systems, Inc., Houston, PA, U.S.A.

(*Received* 25 *August* 1992; *in revised form* 2 *July* 1993)

Abstract—A numerical procedure for the analysis of the stresses due to rotation that are produced in disks of a general, arbitrary configuration is presented in this paper. The governing equilibrium equations and the constitutive relations for the rotating disk element are written in terms of the radial stress. A numerical simulation is performed based on repeated applications of a truncated Taylor's expansion to advance along the radius of the deformed disk. The treatment of both initial value problems and two point boundary value problems is presented based on a corresponding iterative root finding method. Examples for various disk geometries, including disks of constant thickness, linearly tapered thickness, and hyperbolic variation of thickness, respectively, are provided. Both radial as well as circumferential stresses are obtained and compared with existing analytical solutions to validate the present formulations. Particular consideration is given to the industrial example of turbine rotors carrying buckets. The simple procedure developed in this study may serve as an effective tool for performing preliminary design calculations for complex rotating components.

INTRODUCTION

The analysis of rotating components merits attention due to its numerous possible practical applications. Some analytical elasticity solutions for the analysis of rotating disks with simple cross section geometries do exist in the literature, see for example, Love (1944), Timoshenko and Goodier (1970), Saada (1974), and Ugural and Fenster (1987). These simple geometries include axisymmetric disk sections with a constant thickness, a linearly varying thickness, and a hyperbolic varying thickness, respectively.

For an arbitrary geometry, generally, the analysis is carried out by considering the disk to be composed of segments of piecewise constant thickness. The analysis of complex geometries as well as of complex components, such as a turbine rotor with a hub and rim, and buckets along its periphery, is not possible using the existing analytical techniques.

A detailed analysis of a rotating disk with an arbitrary geometry may also be performed using numerical techniques, such as the finite element method, Zienkiewicz (1971), or the boundary element method, Banerjee and Butterfield (1981). The boundary element method is especially advantageous as only the boundary of the axisymmetric model needs to be discretized, Abdul-Mihsein *et al.* (1985). Such detailed analyses, however, usually require an extensive use of computer resources, are tedious to perform due to extensive meshing requirements and are expensive, making them unsuitable for preliminary design type analysis. In contrast, the present numerical formulation is simple and efficient, yet reliable, giving it the potential to be a very effective preliminary design tool.

THEORETICAL FORMULATION

The static equilibrium of a differential element of a rotating disk, treating the centrifugal inertia force as a body force, may be written as:

$$\sigma_r' + \frac{(\sigma_r - \sigma_\theta)}{r} + \frac{t'}{t}\sigma_r + \rho r\omega^2 = 0. \tag{1}$$

The strain displacement relations and the constitutive relations for the axisymmetric cases are combined to give:

$$Eu' = \sigma_r - \upsilon\sigma_\theta, \tag{2}$$

$$\frac{Eu}{r} = \sigma_\theta - \upsilon\sigma_r, \tag{3}$$

where σ_r and σ_θ are the radial and circumferential stresses, respectively; r is the radius; $t = t(r)$ is the thickness; ρ is the mass density; E and υ are the modulus of elasticity and Poisson's ratio, respectively; ω is the angular velocity; u is the radial displacement; and a prime superscript denotes differentiation with respect to r.

The variable σ_θ is eliminated from eqns (1)–(3) and the result, after some manipulations, is written as

$$\sigma_r' = \frac{Eu}{r^2} - \frac{(\lambda - \upsilon)}{r}\sigma_r - \frac{\beta r}{(3+\upsilon)}, \tag{4}$$

and

$$\sigma_r'' = \frac{-(\lambda+2)}{r}\sigma_r' - \frac{[r\lambda' + (\lambda-1)(1+\upsilon)]}{r^2}\sigma_r - \beta, \tag{5}$$

where $\lambda = 1 + (rt'/t)$; and $\beta = (3+\upsilon)\rho\omega^2$.

NUMERICAL FORMULATION

The solution of stresses in a rotating component, such as a turbine rotor, may now be obtained by solving the differential eqns (4) and (5) together with the corresponding boundary conditions. To obtain a solution to these equations, the radial stress is expressed, using a truncated Taylor's expansion, as

$$\sigma_r(s+\Delta s) = \sigma_r(s) + \sum_{n=1}^{N}\left[\frac{\partial^n\sigma_r(s)}{\partial s^n}\right]\frac{(\Delta s)^n}{n!}, \tag{6}$$

where s is the distance along the radius of the rotating disk, Δs is the corresponding increment in distance, and N is the number of terms carried in the Taylor's expansion.

For the cases which can be expressed as initial value problems, the simulation begins at $s = 0$ where the boundary conditions are known. The simulation is then advanced through an increment Δs using eqn (6) where the derivatives $\partial^n\sigma_r(s)/\partial s^n$ are obtained from eqns (4) and (5). The higher order derivatives for σ_r required in eqn (6) are obtained through successive differentiations of eqn (5).

For two point boundary value problems, the simulation is started with a trial value for the missing boundary condition at $s = 0$. The simulation is then carried out to the position along the radius of the disk where the other boundary condition is known. The difference between the desired boundary condition and that which was obtained through simulation is treated as a vector function of the trial value. An iterative root finding procedure is incorporated which necessitates repeated simulation passes until the boundary conditions at the two end points are simultaneously satisfied. A similar root-finding procedure has been used earlier for the solution of elastica problems, Saigal and Kistler (1989).

It is noted that the circumferential stress, σ_θ, may be written in terms of the radial stress, σ_r, and its derivatives through a rearrangement of the terms in eqn (1). Thus, once

the radial stress, σ_r (along with its derivatives) has been obtained using the above procedure, the circumferential stress, σ_θ, can be obtained directly from eqn (1).

FORMULATION FOR TURBINE ROTOR

For the turbine rotor consisting of a hub, a web and a rim carrying buckets, as shown in Fig. 8, a two point boundary value problem for the simulation of the web is defined using the boundary conditions for the web at the hub–web and the web–rim interfaces. These interface conditions are first obtained by separately considering the equilibrium of the hub and the rim, respectively.

Rotor hub

The hub of the rotor is of a constant thickness, giving $\lambda = 1$ and $\lambda' = 0$ so that eqn (5) becomes:

$$\sigma_r'' = \frac{-3}{r}\sigma_r' - \beta. \tag{7}$$

The solution for eqn (7) is written as:

$$\sigma_r = \frac{-\beta r^2}{8} - \frac{A_1}{2r^2} + A_2, \tag{8}$$

and from differentiation of eqn (8):

$$\sigma_r' = \frac{-\beta r}{4} + \frac{A_1}{r^3}, \tag{9}$$

where A_1 and A_2 are constants. Equations (8) and (9) may now be substituted into eqn (4). Performing this substitution, and solving for the constants A_1 and A_2 using the boundary conditions for the hub as $\sigma_r\,(R_1) = 0$ and $u(R_2) = u_2$, gives the radial stress at the hub–web interface, after some manipulations, as:

$$\sigma_r(R_2) = A_3(u_2 - A_4) \tag{10}$$

$$A_3 = \frac{(R_2^2 - R_1^2)E}{R_2[(1+\upsilon)R_1^2 + (1-\upsilon)R_2^2]}; \quad A_4 = \frac{R_2\beta}{4E}\left[R_1^2 + R_2^2\frac{(1-\upsilon)}{(1+3\upsilon)}\right],$$

where R_1 is the inner radius of the hub; R_2 is the radius at the hub–web interface; and u_2 is the radial displacement at the hub–web interface.

Rotor rim

The rim of the turbine rotor is assumed to be thin (i.e. its width L_r along the radius is small) so that σ_θ is approximately uniform throughout the rim. Equation (3) then gives:

$$\sigma_\theta = \frac{Eu}{R}, \tag{11}$$

where u is the radial displacement of the rim, and R is the radial location on the rim.

If the total weight of the buckets on the periphery of the rim is W_b, then the centrifugal force acting on the rim due to this weight is:

$$F_b = \frac{W_b}{g}R\omega^2, \tag{12}$$

where g is the acceleration due to gravity. The stress induced in the rim due to W_b is written as:

$$\sigma_b = \frac{F_b}{2\pi Rt}, \tag{13}$$

where t is the thickness of the rim.

Static equilibrium of the rim gives:

$$\sigma_\theta = \frac{R\sigma_b + t\rho R^2\omega^2 - R\sigma_r(R_3),}{t}, \tag{14}$$

where $\sigma_r(R_3)$ is the radial stress at the inside surface of the rim. Combining eqns (11) and (14), and rearranging terms to solve for $\sigma_r(R_3)$, results in the expression:

$$\sigma_r(R_3) = A_5(A_6 - u) \tag{15}$$

$$A_5 = \frac{Et}{R^2}; \quad A_6 = \frac{\beta R^3}{E(3+\upsilon)} + \frac{R^2\sigma_b}{Et}.$$

Equations (10) and (15) are the boundary conditions at the hub–web and the web–rim interfaces, respectively, which define the two point boundary value problem for the simulation of the web. The solution for this problem is obtained in an iterative fashion using the numerical procedure described previously to determine the complete response of the rotor. The iterations are started by assuming a value for the radial displacement, u_2, of the hub–web interface, in eqn (10).

EXAMPLE PROBLEMS AND PRACTICAL APPLICATION

The analysis of a number of rotating disks with constant thickness, linearly tapered thickness, and hyperbolically varying thickness, respectively, along their radial section was carried out to demonstrate the validity of the above formulations. Annular disks, as well as solid disks, rotating at an angular velocity of $\omega = 700$ rad s^{-1} were considered. The material properties of the disks were assumed as: $E = 200 \times 10^9$ Pa, $\rho = 7800$ kg m^{-3}, and $\upsilon = 0.3$. Both the annular disks and the solid disks were studied under two distinct loading conditions: (a) no load $Q = 0$ applied to the disk, and (b) a uniform load, $Q = 65$ MPa, applied at the outer periphery of the disk.

For both loaded and unloaded annular disks, respectively, a step length, $\Delta s = 1.0 \times 10^{-3}$ m, was used, resulting in a total of 200 equal steps. The solution for the radial stress distribution of an annular disk was considered to have converged when, at the outer rim, $|Q - \sigma_r| \leqslant$ TOL was satisfied, where TOL is a prespecified tolerance. A value of TOL $= 1.0 \times 10^{-6}$ Pa was used for the annular disk examples.

For the stress analysis of a solid disk, the disk was divided into 2500 equal steps of length $\Delta s = 1.0 \times 10^{-4}$ m. Convergence was considered to be achieved when $|u_0| \leqslant$ TOL, where u_0 is the radial displacement at the center of the solid disk. A value of TOL $= 1.0 \times 10^{-20}$ m was specified for both load cases.

For all the disk examples considered in this study, the analysis was repeated using a step length of $\Delta s/2$ and the same results were obtained as with a step length of Δs indicating a convergence of the solution with respect to the step length.

Disks with constant thickness

A rotating annular disk with a constant thickness was first considered. The radial and circumferential stress distributions along the radial section of the disk were obtained for both loading conditions mentioned above. The results obtained for these loadings applied to the disk were shown in Fig. 1. The exact analytical solutions for the analysis of annular

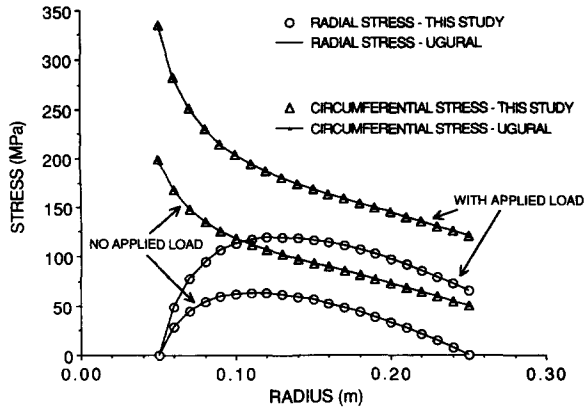

Fig. 1. Stress distributions for an annular disk of constant thickness.

disks of constant thickness are available in Ugural and Fenster (1987). These analytical solutions were also plotted in Fig. 1 for comparison, and an excellent agreement was seen.

The analysis of solid disks of constant thickness was considered next. The radial stress distribution for the two loading conditions mentioned above were plotted in Fig. 2. The exact analytical solution given by Ugural and Fenster (1987) for a solid disk of constant thickness was also shown in Fig. 2 for comparison. As seen in this figure, a good agreement was observed for all locations along the radius of the disk, except at the center, where the radial stress found in this study drops to zero.

Disks with linearly tapered thickness

The analysis of rotating tapered disks, both annular and solid, with the thickness varying linearly along their radius was performed. The thickness of these disks increases from the center of the disk outward, thus reaching its greatest value at the periphery. Although this was recognized as a rather impractical geometry, analytical solutions for comparison were available for only this form of tapered disk. The radial and circumferential stress distributions along the radius of the tapered disk were determined for both the annular disk and the solid disk under each of the load cases described above. The results for the annular and the solid disk are shown in Figs 3 and 4, respectively. The analytical solutions by Saada (1974) for disks with varying thickness were also plotted in these figures. The numerical solutions obtained in this study compare well with the analytical solutions. The only discrepancy observed, as seen in Fig. 4, was in the results for the solid disk with an applied load. The radial stress from this study drops to zero at the center of the disk, while the analytical solution goes to infinity.

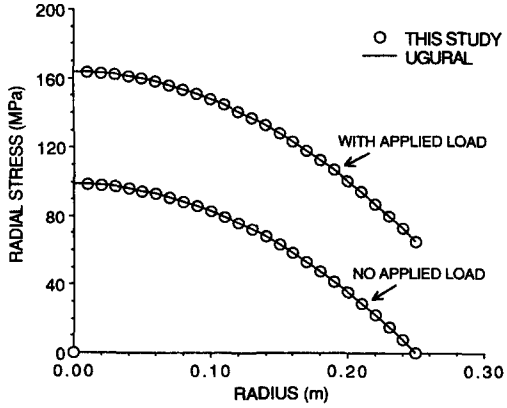

Fig. 2. Radial stress distribution for a solid disk of constant thickness.

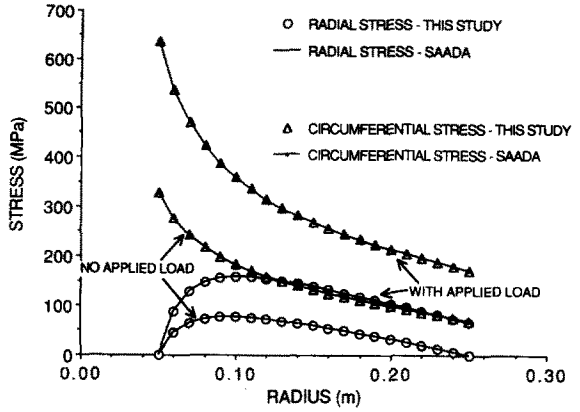

Fig. 3. Stress distributions for an annular disk of tapered thickness.

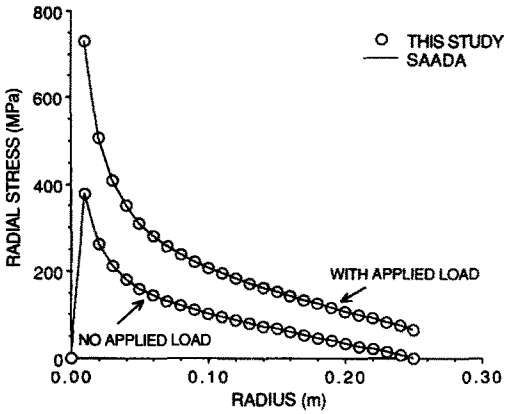

Fig. 4. Radial stress distribution for a solid disk of tapered thickness.

Further analyses were performed on linearly tapered disks with the thickness along the radius decreasing in dimension from the center of the disk outward. This case corresponds to a realistic geometry for tapered disks. The radial stress distributions for an annular disk and a solid disk of this geometry, respectively, are shown in Fig. 5.

Disks with hyperbolic thickness

A rotating annular disk with a hyperbolic variation of thickness along its radius was next investigated under the two loading conditions previously mentioned. The results for

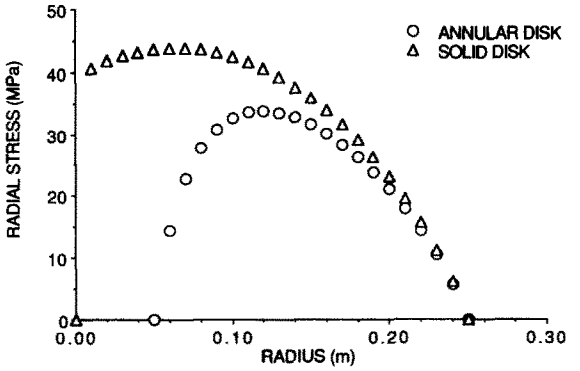

Fig. 5. Radial stress distribution for a disk of tapered thickness decreasing from the center of the disk outward.

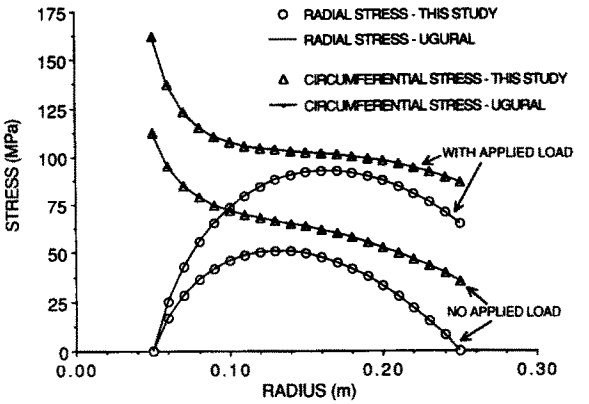

Fig. 6. Stress distributions for an annular disk of hyperbolic thickness.

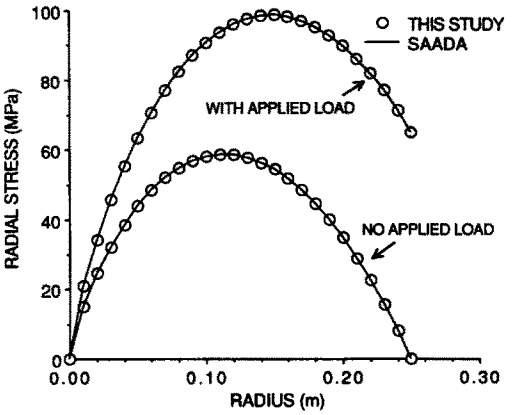

Fig. 7. Radial stress distribution for a solid disk of hyperbolic thickness.

circumferential and radial stress distributions obtained from the present analysis were shown in Fig. 6, along with the analytical solution by Ugural and Fenster (1987) for annular disks of hyperbolic thickness. The radial stress distribution results for a solid hyperbolic disk are presented in Fig. 7 along with the analytical solution by Saada (1974). Excellent agreement between analytical and numerical solutions was observed in each case.

Application to turbine rotors

Finally, the present numerical formulation was used to determine the radial and circumferential stress distributions for the web of a rotating turbine rotor with a hub, web

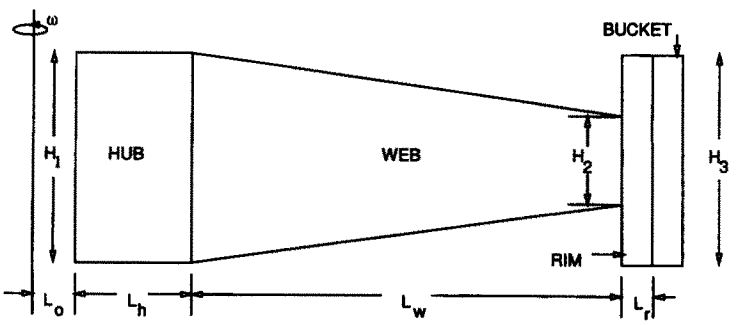

Fig. 8. Cross section geometry of a turbine rotor.

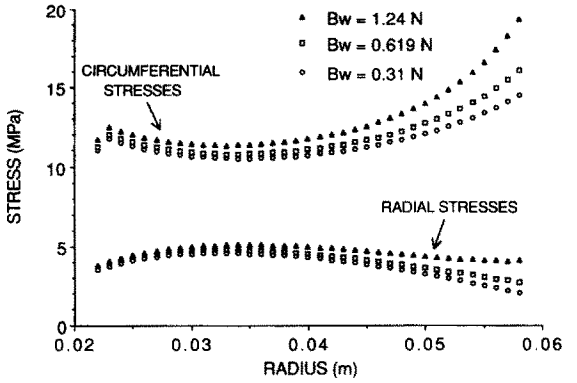

Fig. 9. Stress distributions in the web of a turbine rotor for constant angular velocity and varying bucket weight.

and rim, complete with buckets along the periphery. The geometry of the rotor, shown schematically in Fig. 8, involves a web with linearly tapered thickness along its radial section. The material properties of the rotor were assumed as: $E = 210 \times 10^9$ Pa, $\rho = 8304$ kg m^{-3}, and $\upsilon = 0.3$. The geometric data used was: $L_o = 1.5$ cm, $L_h = 0.7$ cm, $L_w = 3.6$ cm, $L_r = 0.2$ cm, $H_1 = 2.5$ cm, $H_2 = 0.7$ cm, and $H_3 = 1.5$ cm.

A step length $\Delta s = 1.0 \times 10^{-4}$ m was used, resulting in a total of 360 equal steps. The solution was considered to have converged when $|\sigma_{ro} - \sigma_{ri}| \leqslant$ TOL was satisfied, where σ_{ro} is the radial stress at the outer radius of the web and σ_{ri} is the radial stress at the inner radius of the rim. A value of TOL $= 1.0 \times 10^{-10}$ Pa was used for this example. The same results were also obtained at smaller values of Δs, thus establishing convergence with respect to step length.

The turbine rotor was first analyzed keeping the angular velocity $\omega = 1050$ rad s^{-1} constant, and varying the weight of the buckets W_b as 0.31 N, 0.619 N, and 1.24 N, respectively. The results of the analyses are shown in Fig. 9.

The rotor was analyzed again with a constant $W_b = 0.619$ N, and varying ω as 1050 rad s^{-1}, 1500 rad s^{-1}, and 2000 rad s^{-1}, respectively. The solutions for the analyses are shown in Fig. 10.

CONCLUSIONS

This paper presents a numerical procedure for the analysis of the radial and circumferential stresses produced in rotating components, including disks of constant thickness, linearly tapered thickness, and hyperbolic thickness, respectively. The governing

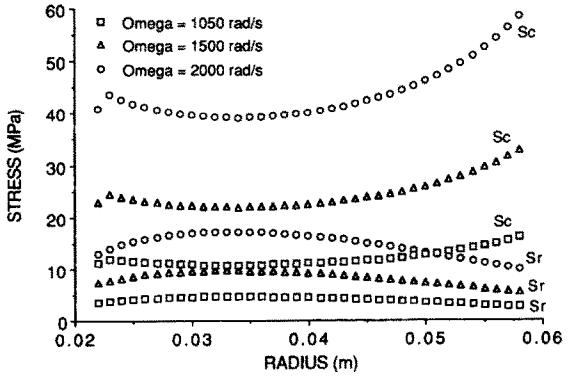

Fig. 10. Stress distributions in the web of a turbine rotor for constant bucket weight and varying angular velocity. Sc = Circumferential Stress, Sr = Radial Stress.

equilibrium and constitutive equations for the rotating component are written in terms of the radial stress. A truncated Taylor's series is repeatedly applied in order to advance along the radius of the rotating component, and an interative root finding method is utilized to solve both initial value problems and two point boundary value problems. Numerical solutions obtained in this study show a close agreement with the analytical solutions, demonstrating the validity of the formulations as well as the solution procedures used. A significant achievement in this study is that this simple procedure can be used successfully to analyze components of arbitrary geometry and complex arrangements, such as a turbine rotor with a hub, web and rim carrying buckets, whose analysis is not possible with existing analytical techniques and whose analysis using alternative numerical techniques is too cumbersome and expensive. The present numerical approach can be employed effectively for obtaining the stress distributions of complex rotating components, thus constituting a valuable tool for preliminary design analysis.

Acknowledgements—This work was supported by a Small Undergraduate Research Grant (SURG) from ARCO Chemical Company and the Lily Endowment, Inc. and by the National Science Foundation through a supplement grant MSM9057055 to Carnegie Mellon University.

REFERENCES

Abdul-Mihsein, M. J., Bakr, A. A. and Parker, A. P. (1985). Stresses in axisymmetric rotating bodies determined by the boundary integral equation method. *J. Strain Anal.* **20**(2), 79–86.

Banerjee, P. K. and Butterfield, R. (1981). *Boundary Element Methods in Engineering Science*. McGraw-Hill, New York.

Love, A. E. H. (1944). *A Treatise on the Mathematical Theory of Elasticity*. Dover Publications, New York.

Saada, A. S. (1974). *Elasticity Theory and Applications*. Pergamon Press, New York.

Saigal, S. and Kistler, W. A. (1989). A direct vector simulation for the analyses of nodal and undulating elastica. *Int. J. Solids Structures* **25**(2), 201–211.

Timoshenko, S. P. and Goodier, J. N. (1970). *Theory of Elasticity*. 3rd Edition, McGraw-Hill, New York.

Ugural, S. C. and Fenster, S. K. (1987). *Advanced Strength and Applied Elasticity*. Elsevier, New York.

Zienkiewicz, O. C. (1971). *The Finite Element Method in Engineering Science*. McGraw-Hill, London.